Charge and spin ordering process in the mixed-valence system $LuFe_2O_4$: Charge ordering

Y. Yamada, K. Kitsuda, S. Nohdo, and N. Ikeda
Advance Research Center for Science and Engineering, Waseda University, Okubo, Tokyo 169-0072, Japan
(Received 3 April 2000)

The charge ordering process in a mixed valence system $LuFe_2O_4$ is investigated both experimentally and theoretically. The experimental results using various types of diffraction techniques reveal the following unique features. (i) The system undergoes sequential transitions: disorder→2D-CDW→3D-CDW. (ii) The structure stabilized in the lowest temperature is characterized by an incommensurate charge-density-wave (CDW) state. (iii) In the intermediate temperature range, there appear strong diffuse streaks running along the rhombohedral unique axis which show subtle zig-zag modulation. These experimental results are analyzed based on the assumption that the ordering charges are essentially localized on Fe sites. The energy between the electron pairs up to the nearest-neighbor hexagonal double layers are taken into account to discuss the stable charge configuration and the properties of charge fluctuations. It has been shown that the experimentally observed unique features of the charge ordering process are satisfactorily explained only when the intercharge interaction between the neighboring layers is taken to be attractive.

I. INTRODUCTION

$LuFe_2O_4$ belongs a class of materials generally expressed by RFe_2O_4 (R indicates rare-earth metals).[1] The crystals of these materials belong to the rhombohedral system (space group $R\bar{3}m$) (Ref. 2) and have the following characteristic properties: (i) In these crystals, Fe ions are arranged to form the hexagonal double layers and stack in the sequence of $(AB),(CA),(BC),\ldots$ along the rhombohedral unique axis [See Fig. 1(a)]. (ii) The average valence of Fe ions is $Fe^{2.5+}$, which implies that Fe^{2+} and Fe^{3+} ions occupy the equivalent Fe sites on the hexagonal net plane with equal probability when averaged out.

These features lead to an interesting characterization of these materials to be a charge-spin frustrated system. The aspect of spin frustration has been noticed earlier[3–6] and various experimental studies have been carried out. The aspect of charge frustration was later pointed out by Ikeda and co-workers in connection with the anomalous dielectric behavior in this class of materials.[7–9]

The formal similarity of spin frustration and charge frustration is explained in Fig. 1(b). Suppose one tries to arrange an equal number of the excess charge of Fe2+ (represented by the black site) and the excess hole (represented by the white site) on the hexagonal lattice. The common nearest-neighbor site adjacent to a black and white pair is frustrated as symbolically represented by the gray site in the figure, which means that the ground state of the system tends to be degenerated.

The frustration or the degeneracy of the ground state would affect the charge-spin ordering process in these materials to exhibit somewhat unique features, in particular in the properties of fluctuations of the order parameters.

The purpose of the present study is to carry out experimental investigations on the ordering process in $LuFe_2O_4$ in both the charge system as well as in spin system with emphasis on the properties of the charge-spin fluctuation, in order to elucidate the microscopic interactions acting between charges and spins. In this paper (Part I), we focus our attention on the charge ordering process. In Sec. II, the experimental results are presented. Based on the theoretical treatment developed in Sec. III, the experimental results are analyzed in Sec. IV. Section V is devoted to the summary and discussions. A preliminary report of the present work has been published elsewhere.[10]

II. EXPERIMENTAL

Various types of diffraction techniques have been utilized in the present experiment. Single-crystal samples were provided by S. Kito of the Electrochnical Laboratory using the FZM method. Details of growing single crystals were reported elsewhere. The 200 keV electron microscope JEM-200CX installed at the *Y* amamoto Laboratory, Tokyo Institute of Technology, was utilized to obtain the overall features of the diffraction characteristics of this material. On the other hand, x-ray-diffraction experiments were carried out at Noda Laboratory, Chiba University, with a four-circle-type diffractometer and Mo $K\alpha$ radiation. Neutron-diffraction studies were performed at the JRR-3 reactor, Japan Atomic Energy Research Institute. The triple-axis-type spectrometers were mainly utilized. In contrast to the electron-diffraction measurements, the x-ray and neutron-diffraction results provided more detailed informations on the diffraction characteristics throughout a wide temperature range of $4\,\mathrm{K}<T<550\,\mathrm{K}$.

(i) $320\,\mathrm{K}<T\lesssim 500\,\mathrm{K}$. In this temperature region, the electron-diffraction pattern in $(h\,h\,l)$ reciprocal plane (in this paper, we use the hexagonal index instead of the rhombohedral index corresponding to the space group $R\bar{3}m$) exhibits the following characteristic features: As is shown in Fig. 2 of Ref. 10, in addition to the fundamental Bragg reflections indexed by $(h\,h\,3l)$, there appear strong diffuse streaks running along the c^* axis on $(h\pm 1/3\,k\pm 1/3\,l)$. However, with a more detailed observation of the electron-diffraction pattern, one notices that the diffuse lines show systematic subtle zig-zag behavior.

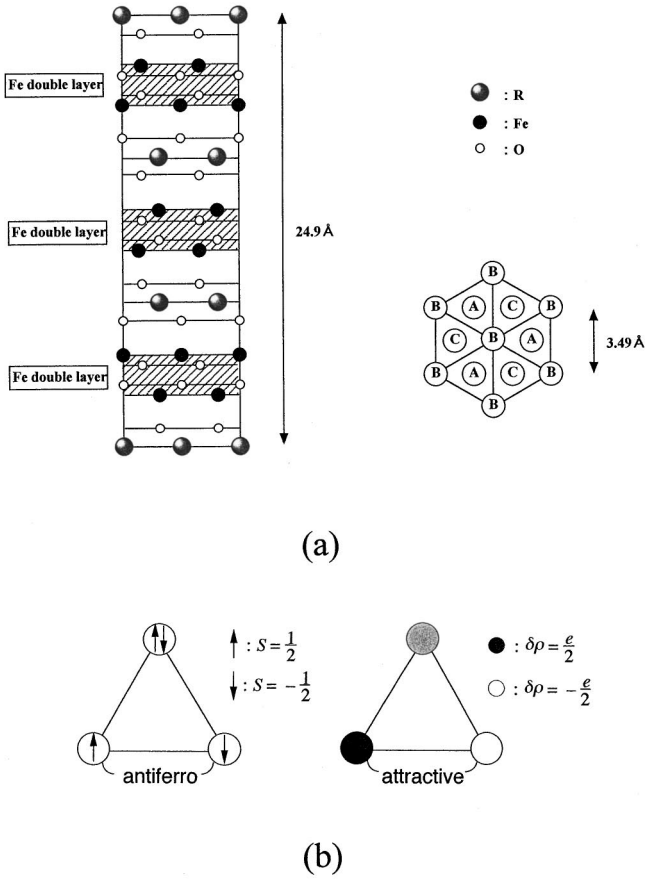

FIG. 1. (a) Schematic description of the crystal structure of $R\mathrm{Fe_2O_4}$ belonging to space group $R\bar{3}m$. Fe ions form the hexagonal double layer such as (A,B) which are sandwiched by (Lu, O) blocks and stacked along the rhombohedral unique axis in the sequence of (AB), (CA), (BC). (b) Spin frustration vs charge frustration on a 2D hexagonal lattice. The common nearest-neighbor site for the ($\uparrow-\downarrow$) pair (black and white pair) has no preference of $\uparrow$ or $\downarrow$ (black or white) since the energy is completely degenerated. This situation is expressed by the gray site in the case of charge frustration.

(ii) $T<320$ K. As the temperature is lowered below 320 K, the diffuse streaks start to condense to give discrete satellite reflections. The x-ray-diffraction pattern around (1/3 1/3 l) observed at $T=270$ K is given in Fig. 2(a). It is noticed that the satellites are not on the exact (1/3 1/3 l) line, but show small shifts along the [h h 0] direction, resulting in similar zig-zag behavior to the diffuse streak observed at $T>320$ K. In the figure, we have expanded the horizontal axis ([110] axis) by a factor of 10 compared with the actual c^*/a^* ratio in order to demonstrate the shifts clearly. Figure 2(b) gives the detailed diffraction pattern in the actual reciprocal space. There are diffuse streaks still remaining which seem to connect the satellite reflections. Detailed analysis of the satellite positions shows that series of satellite reflections are consistently indexed by considering small incommensurability δ from (1/3 1/3 l) as follows:

$$(h\ \ h\ \ l)+(1/3(1+\delta),1/3(1+\delta),3/2):l=3n,$$

$$(h\ \ h\ \ l)+(-2/3(1+\delta),1/3(1+\delta),3/2):l=3n+1,$$

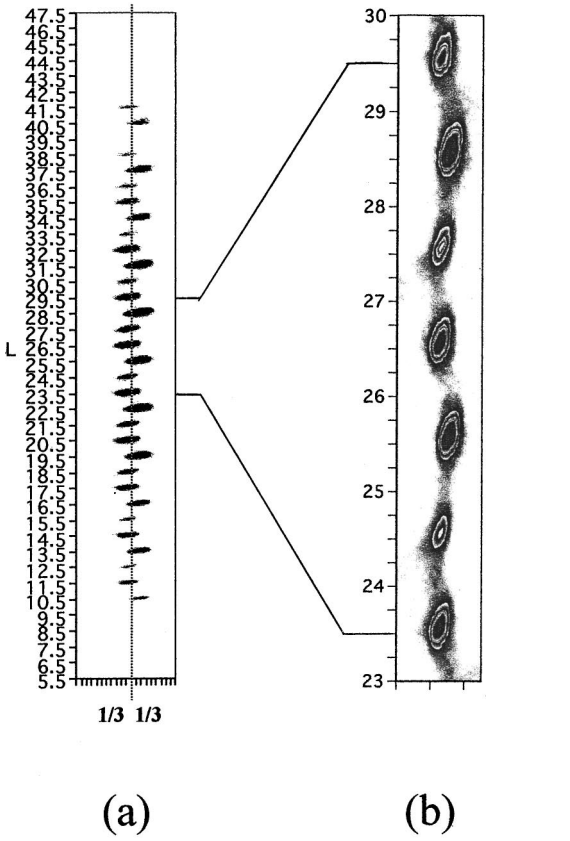

FIG. 2. (a) Observed x-ray-diffraction pattern around (1/3 1/3 l) at $T=270$ K. The satellite reflections are indexed by the incommensurate values. In order to demonstrate the incommensurability clearly, the horizontal [1 1 0] axis is expanded by a factor of 10 compared with the actual c^*/a^* ratio. (b) Detailed x-ray-diffraction pattern within $l=23-30$ in the actual c^*/a^* ratio. There are still some diffuse streaks remaining connecting between the neighboring satellite reflections.

$$(h\ \ h\ \ l)+(1/3(1+\delta),-2/3(1+\delta),3/2):l=3n-1,$$

$$\delta=0.0081. \tag{1}$$

Notice the satellites for $l=3n\pm1$ are slightly off from the exact (h h l) reciprocal plane. This feature is manifested in the fact that the intensities of these satellites are systematically weaker than those for $l=3n$ [See Fig. 2(a)].

In addition, another type of satellite pair appears in the same temperature range having the indices

$$(h\ \ h\ \ l)\pm(\delta',\delta',1/2)\quad(l=3n).$$

$$\delta'=0.030. \tag{2}$$

The profile of the satellite pairs around (0 0 22.5) observed by x-ray scanning through the [h h 0] line is given in Fig. 3.

The overall diffraction characteristic at $T<320$ K is given schematically in Fig. 6(b) of Ref. 10. The pattern clearly demonstrates that below $T_c=320$ K, three-dimensional 3D ordering has been developed where the order parameter exhibits incommensurate modulation in the space.

Since T_c just corresponds to the critical point where the dielectric constant shows anomalous behavior, we infer that the transition is associated with the charge ordering process

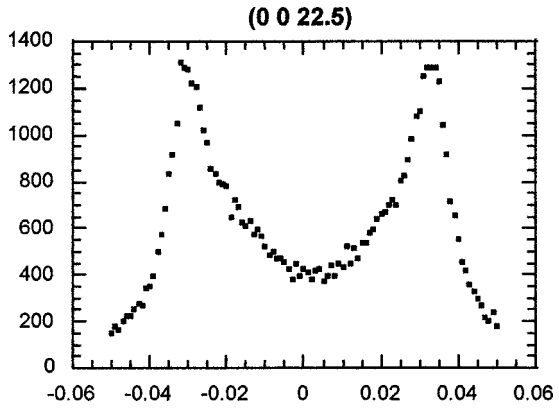

FIG. 3. Observed x-ray intensity profile around (0 0 13.5) scanned along [1 1 0] direction at $T=300$ K. The satellite pair is indexed by $(0\ 0\ 13)\pm(\delta'\,\delta'\,1/2)$, $\delta'=0.030$.

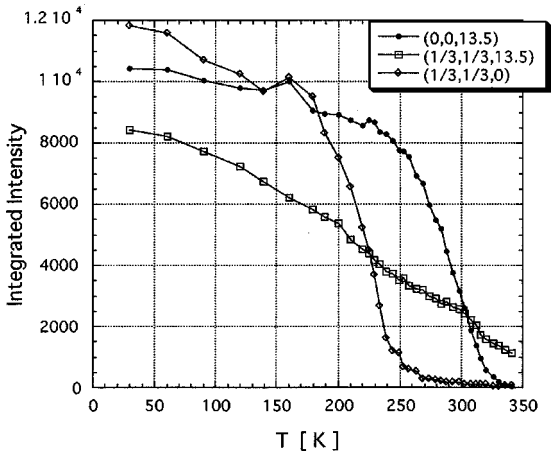

FIG. 4. Temperature dependences of the integrated intensities of the satellite reflections. In the figure the magnetic reflection (1/3 1/3 0) is also included which will be discussed in the second part of the paper.

of Fe ions, and identify the order parameter to be the local charge density on the Fe site. Although x-ray diffraction is not an effective probe to observe the valence electron density, a change in valence electron configuration at the Fe ion inevitably introduces displacements of the neighboring oxygens to form small polarons. In this context, x-ray as well as neutron diffraction is effectively detecting the charge ordering through small lattice distortions associated with the polaron ordering.

Temperature variations of the integrated intensities of the satellites observed by neutron diffraction are shown in Fig. 4. The satellite reflection $[1/3(1+\delta),\ 1/3(1+\delta),\ 13.5]$ shows only a slight change at $T_c(=320\ \mathrm{K})$. The remanent intensity above T_c is due to the strong diffuse streak intensity, which gradually decreases to disappear around $T\sim 500$ K. We interprete that in the temperature range of $320\ \mathrm{K}<\mathrm{T}<500$ K, only the short-range order of the charge density develops. However, since the intralayer correlation length is so large as compared with the interlayer correlation length, the state in this temperature range may be characterized by a 2D ordered state in hexagonal basal plane. On the other hand, the integrated intensity at $(\delta',\delta',13.5)$ starts to appear at $T_c=320$ K showing characteristics of ordinary 3D cooperative ordering. Summarizing, the phase transition scheme in $LuFe_3O_4$ is viewed as shown in the following diagram.

IC 3-D CDW	2-D CDW	Disorder
	320K	500K

In the 2-D ordered state, the wave vector, $\mathbf{k}^{(2D)}$, of the charge density wave is given by $\mathbf{k}^{(2D)}=(1/3\ 1/3)$ if we assume that the streak is running exactly parallel to the c^* axis. In this approximation, we may visualize the system to be a random stacking of charge ordered hexagonal layer where the in-plane charge-density wave (CDW) is characterized by the wave vector $\mathbf{k}^{(2D)}=(1/3\ 1/3)$. In the 3D ordered state, the charge-density wave is characterized by the wave vector $\mathbf{k}=[1/3(1+\delta),1/3(1+\delta),3/2]$ with $\delta=0.081$. The other types of satellite reflections at $(h\ h\ l)\pm(\delta',\delta',1/2)$ are considered to be a higher-order effect corresponding to the third-order harmonic which has the wave vector $\mathbf{k}'=3\mathbf{k}$.

III. THEORY

As is described in the preceding section, $LuFe_2O_4$ exhibits the phase-transition scheme associated with the charge ordering which shows the following rather unique features.

(i) It undergoes sequential transitions: disorder→2D-CDW→3D-CDW.

(ii) The ground state stabilized in low temperatures is characterized by incommensurate CDW state.

(iii) In the intermediate temperatures, the diffraction pattern exhibits peculiar zig-zag diffuse streaks.

In order to elucidate the physical origin of these features, we investigate theoretically the thermodynamical properties of the mixed-valence system based on the assumption that the valence electrons are essentially localized on Fe sites.

We start with setting up the Hamiltonian given by the potential energy between the excess electrons and holes relative to the average valence of $+2.5$ on the Fe sites as follows:

$$H=\sum J_{ij}^{\upsilon\upsilon'}\cdot S_i^{\upsilon}S_j^{\upsilon'},\quad \upsilon=1,2. \tag{3}$$

Here the variable S_i^{υ} takes on

$$S_i^{\upsilon}=\begin{cases} 1 & :\text{when the } \nu \text{ site in the } i\text{'s unit cell is occupied by the } Fe^{2+} \text{ ion,}\\ -1 & :\text{when the } \nu \text{ site in the } i\text{'s unit cell is occupied by the } Fe^{3+} \text{ ion,}\end{cases}$$

and $J_{ij}^{\nu\nu'}$ is the interaction between the pair of electrons/holes on (i, ν) and (j, ν') site. Notice there are two Fe sites in the primitive rhombohedral unit cell: Fe (I) at (0 0 0) and Fe (II) at (1/2 1/2 1/2), so that ν takes on 1 or 2.

By defining the Fourier transforms

$$S^{\nu}(\mathbf{k}) = 1/\sqrt{N} \sum_i S_i^{\nu} e^{i\mathbf{k}\cdot\mathbf{r}_i},$$

$$J^{\nu\nu'}(\mathbf{k}) = 1/\sqrt{N} \sum_j J_{ij}^{\nu\nu'} e^{i\mathbf{k}\cdot\mathbf{r}_{ij}}, \tag{4}$$

the Hamiltonian is rewritten as

$$H = \sum_k \mathbf{S}^{+}(\mathbf{k}) \cdot \mathbf{J}(\mathbf{k}) \cdot \mathbf{S}(\mathbf{k}). \tag{5}$$

Here, $\mathbf{S}(\mathbf{k})$ is the column vector,

$$\mathbf{S}(\mathbf{k}) = \begin{pmatrix} \mathbf{S}^{(1)}(\mathbf{k}) \\ \mathbf{S}^{(2)}(\mathbf{k}) \end{pmatrix}, \tag{6}$$

and $\mathbf{J}(\mathbf{k})$ is the (2×2) matrix given by

$$\mathbf{J}(\mathbf{k}) = \begin{pmatrix} \mathbf{J}^{11}(\mathbf{k}) & \mathbf{J}^{12}(\mathbf{k}) \\ \mathbf{J}^{21}(\mathbf{k}) & \mathbf{J}^{22}(\mathbf{k}) \end{pmatrix}, \tag{7}$$

Following the conventional diagonalization procedure, we have

$$H = \sum_k \sum_{\sigma} J^{\sigma}(\mathbf{k}) |S^{\sigma}(\mathbf{k})|^2, \tag{8}$$

$$S^{\sigma}(\mathbf{k}) = \sum_{\nu} C_{\nu}^{\sigma}(\mathbf{k}) \cdot S^{\nu}(\mathbf{k}) \quad (\sigma = 1,2). \tag{9}$$

Here, $J^{\sigma}(\mathbf{k})$ is the energy eigenvalue and $S^{\sigma}(\mathbf{k})$ is the corresponding normal mode of the charge distribution specified by the branch index σ and the wave vector $\mathbf{k}$.

Following the well-known thermodynamical treatment within the random-phase approximation (RPA), we expect the cooperative ordering in $\{S_i^{\nu}\}$ system to take place at the transition temperature T_c given by

$$T_c = J^{\lambda}(\mathbf{k}_0)/k_B, \tag{10}$$

where $J^{\lambda}(\mathbf{k}_0)$ is the lowest energy eigenvalue. The ordered configuration stabilized below T_c is given by the normal modes $S^{\lambda}(\mathbf{k}_0)$ corresponding to the eigenvalue $J^{\lambda}(\mathbf{k}_0)$.

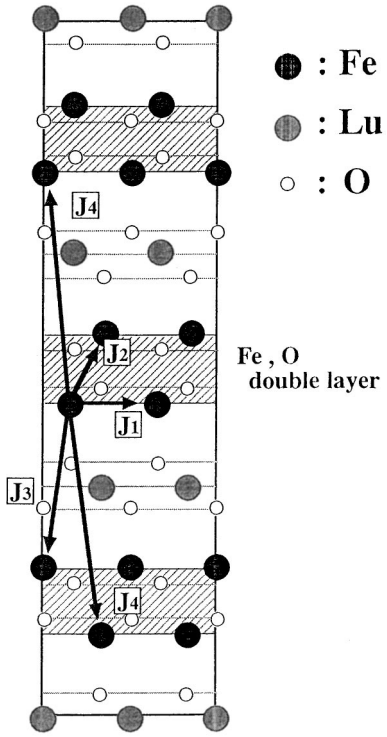

FIG. 5. Effective interactions between charges taken into account in the present treatment. Further interactions are neglected because the dielectric medium should effectively screen the bare Coulombic interaction.

Thus, given the set of the interaction parameters $\{J_{ij}^{\mu\nu}\}$, we can infer the stable charge pattern as follows:

$$S_i^{\nu} = \hat{S} C_{\nu}^{\lambda} e^{i\mathbf{k}_0\cdot\mathbf{r}_i}, \tag{11}$$

where $\hat{S}$ is the amplitude of the order parameter and $C_{\nu}^{\lambda}(\mathbf{k}_0)$ is the νth component of the normal coordinate specified by $(\mathbf{k_0}, \lambda)$.

In the following, we take into account the interactions up to the fourth neighbor as illustrated in Fig. 5. As is seen in the figure, J_1 and J_2 are interactions within the double layer, while J_3 and J_4 give the interactions between the neighboring double layers. Obviously, the existence of the inter-double-layer interactions such as J_3 and J_4 are necessary to achieve a 3D ordered state.

(i) $J_4 = 0$. To proceed stepwise, we first consider the case when $J_4 = 0$. The matrix elements of the $\mathbf{J}(\mathbf{k})$ matrix are given explicitly by

$$J^{11}(\mathbf{k}) = J^{22}(\mathbf{k}) = J_1\{\cos 2\pi(h+k) + \cos 2\pi h + \cos 2\pi k\},$$

$$J^{12}(\mathbf{k}) = J^{21*}(\mathbf{k}) = J_2\{\exp 2\pi i(1/3h + 2/3k - 1/3l) + \exp 2\pi i(-2/3h - 1/3k - 1/3l) + \exp 2\pi i(1/3h - 1/3k - 1/3l)\}$$

$$+ J_3\{\exp 2\pi i(2/3h + 1/3k - 2/3l) + \exp 2\pi i(-1/3h + 1/3k - 2/3l) + \exp 2\pi i(-1/3h - 2/3k - 2/3l)\}. \tag{12}$$

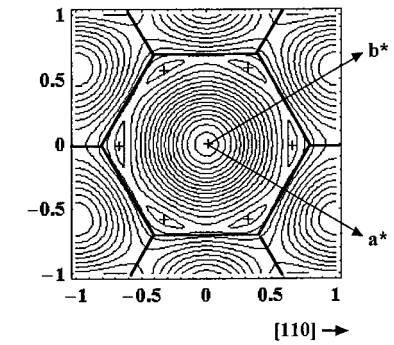

(a)

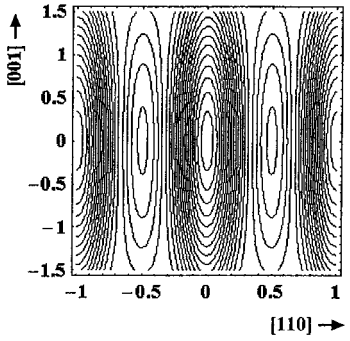

(b)

FIG. 6. (a) Contours of the energy eigenvalues $J^{\lambda}(\mathbf{k})$ belonging to the lowest energy branch in the $(h\,k\,0)$ reciprocal plane in the case of $J_4=0$. It is seen that the minima are located at (1/3 1/3 0) and its equivalent points (+ marks). The thick lines correspond to the Brillouin-zone boundaries of the rhombohedral lattice. (b) Contour map of $J^{\lambda}(\mathbf{k})$ in the $(h\,h\,l)$ plane. It is seen that the contour line around $(1/3\,1/3\,l)$ is running straight along the [0 0 1] direction. The energy is completely degenerated on $\mathbf{k}=(1/3\,1/3\,l)$ [See Fig. 7(e)].

By solving the eigenvalue equations, we have the analytic expression of the energy eigenvalues of the lower branch, $J^{\lambda}(\mathbf{k})$, as a function of $\mathbf{k}$. Figure 6 shows the mapping of the energy contours of $J^{\lambda}(\mathbf{k})$ in the reciprocal planes: (a) $(h\,k\,0)$ plane and (b) $(h\,h\,l)$ plane.

From Fig. 6(a), we see that in the $(h\,k\,0)$ plane the energy minima are at (1/3 1/3 0) and the equivalent points $(-3/2,$ 1/3, 0) and (1/3, $-2/3,$ 0) produced by the symmetry operations of point group $\bar{3}m$. Moreover, from Fig. 6(b), we notice that the contours are running straight along the $(0\ 0\ l)$ line around $(1/3\ 1/3\ l)$, which shows that the stable state is degenerated, being given by the CDW with $\langle 1/3\ 1/3\ l\rangle$ irrespective of the value of l. Physically, this implies that while the in-plane order within the hexagonal double layer is uniquely determined, the stacking sequence remains completely disordered even though the interlayer interaction J_3 is taken into account.

(ii) $J_4\neq 0$. We proceed to include the interaction J_4. It is seen that the complete degeneracy along the $(1/3\,1/3\,l)$ is now lifted. The energy minimum point is given either at $[1/3(1+\delta),1/3(1+\delta),3/2]$ or $[1/3(1-\delta'),1/3(1-\delta'),2/3]$ depending on $J<0$ (attractive) or $J>0$ (repulsive), respectively, [Fig. 7(e)]. The value of $\delta(\delta')$ is dependent on the choice of the parameter value $|J_4|/J_1$.

It is remarkable that the observed satellite positions given in Eq. (1) definitely indicate that the attractive interaction $(J_4<0)$ should be adopted. Figure 7 shows the contrasting energy contours for both $J_4\leqslant 0$ cases. It is interesting that the ditch of the energy contours around the (1/3 1/3 l) line now starts to show zig-zag behavior. This point will be discussed later in more detail.

Making use of the lowest energy eigenvalue, it is easy to find the most stable charge density pattern as follows:

$$\rho^{(1)}(\mathbf{r})=\overline{\rho}e^{i\mathbf{k}_0\cdot\mathbf{r}_i+\phi},$$
$$\rho^{(2)}(\mathbf{r})=-\overline{\rho}e^{i\mathbf{k}_0\cdot\mathbf{r}_i+\phi},$$

$$\mathbf{k}_0=[1/3(1+\delta),1/3(1+\delta),3/2], \tag{13}$$

where ϕ is the phase factor of the wave at the Fe site which is left undetermined in the present treatment. The local pattern of the charge distribution in the real space corresponding to the CDW given in Eq. (13) is depicted in Fig. 8. It is characterized by the arrangement of Fe chains running along the $[1\ \bar{1}\ 0]$ direction in the successive order of Fe^{2+}, Fe^{3+}, $Fe^{2.5+}$,... in the [1 1 0] direction. Notice in more extended regions, the discommensurations (phase solitons) are introduced regularly with the interval of $(3/\delta)$ $\times$(spacing between the neighboring chains) due to the incommensurability δ.

IV. ANALYSIS OF THE EXPERIMENTAL RESULTS

In this section, we analyze the experimental results based on the theoretical treatments developed in the preceding section.

A. Long-range polaron order

As is stated in Sec. II, the satellite reflections observed by x rays as well as neutrons are due to the small displacements of the constituent ions from the high-symmetry positions, which are inevitably introduced upon ordering of charges. In this context, the phase transition is more precisely characterized by the polaron ordering rather than the ordering of bare charges. The pattern of the displacement field should be compatible with the charge pattern of the charge-density wave. Hence, the displacement, $\mathbf{u}_i^{\mu}$ of the μth ion in the ith unit cell accompanying the CDW with the wave vector $\mathbf{k}_0$ should be expressed in terms of the LDW (lattice distortion wave) with the same wave vector of the CDW, as follows:

$$\mathbf{u}_i^{\mu}=\sum_{\kappa} Q_{\kappa}\mathbf{e}_{\mu}^{\kappa}e^{i\mathbf{k}_0\cdot\mathbf{r}_i}, \tag{14}$$

where $\mathbf{e}_{\mu}^{\kappa}$ is the normal coordinate of the κth local vibrational mode to construct the polaron, such as the breathing mode, Jahn-Teller mode, etc., and Q_{κ} is the amplitude of the mode.

The scattering intensity $I(\mathbf{K})$ due to the displacement field $\{\mathbf{u}_i^{\mu}\}$ is given by

$$\mathbf{I}(\mathbf{K})=|F(\mathbf{K})|^2\delta(\mathbf{k}-\mathbf{K}_h\pm\mathbf{k}_0), \tag{15}$$

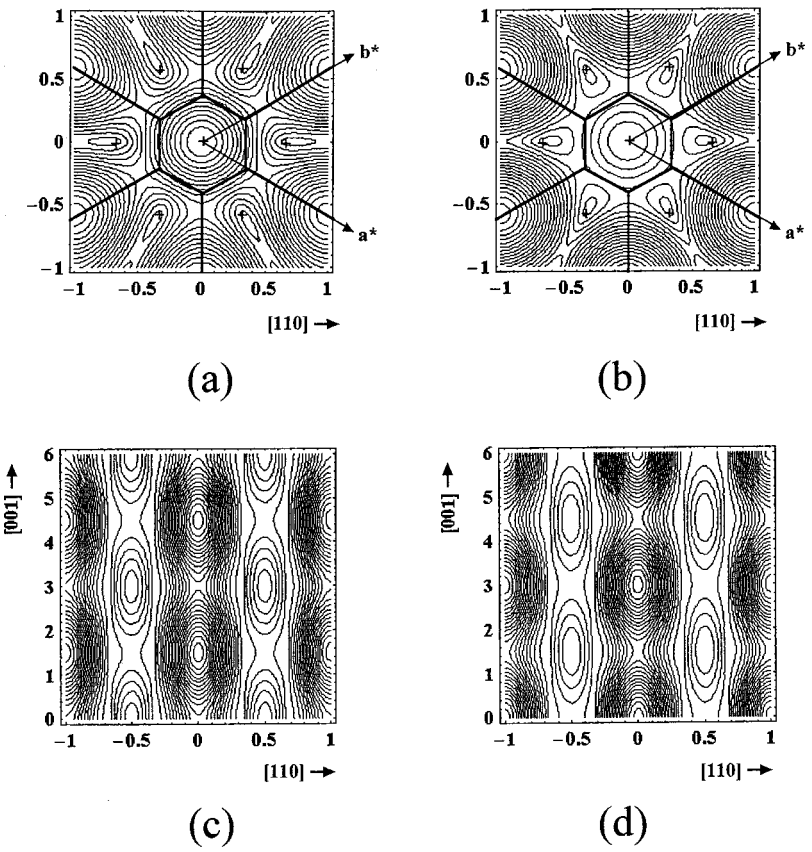

FIG. 7. (a) Contours of the energy eigenvalues $J^\lambda(\mathbf{k})$ in the $(h\ k\ 3/2)$ plane in the case of $J_4<0$. It is seen that the minima are located at $(1/3+\delta,1/3+\delta,3/2)$ and its equivalence. (b) In contrast to (a) $J^\lambda(\mathbf{k})$ in the $(h\ k\ 3/2)$ plane is plotted in the case of $J_4>0$. The minima are located at $(1/3-\delta',1/3-\delta',3/2)$. (c) Contours of $J^\lambda(\mathbf{k})$ in the $(h\ h\ l)$ plane in the case of $J_4<0$. It is seen that the contours are modulated along the [1 1 0] direction thus exhibiting zig-zag behavior along the [0 0 1] direction. (d) In contrast to (c), $J^\lambda(\mathbf{k})$ is plotted in the case of $J_4>0$. The zig-zag pattern is just out of phase to the case of $J_4<0$. (e) The minimum energy values of $J^\lambda(\mathbf{k})$ around $(1/3\ 1/3\ l)$ are projected on the [0 0 1] line. The dashed and solid lines correspond to the case of $J_4=0$ and $J_4\lesssim 0$ respectively. The experimental results are definitely consistent with the case of $J_4<0$.

$$\mathbf{F}(\mathbf{K})=\sum_{\kappa}\sum_{\mu}\mathbf{e}_{\mu}^{\kappa}\cdot Q_{\kappa}e^{i\mathbf{k}\cdot\mathbf{r}_{\mu}}, \tag{16}$$

$$\mathbf{K}_h=H\mathbf{a}^*+K\mathbf{b}^*+L\mathbf{c}^*, \tag{17}$$

where $\mathbf{K}_h$ is the fundamental Bragg positions and $F(\mathbf{K})$ is the polaron structure factor.

In principle, we could determine the structure of the polaron ordered phase by comparing the observed satellite intensities with $\mathbf{I}(\mathbf{K})$ given by Eq. (15), where $\mathbf{e}_{\mu}^{\kappa}$ and Q_{κ} are considered as the disposable parameters to be fixed by a least-square fitting procedure. However, since there are too many disposable parameters included, we satisfy ourselves by examining the satellite positions in the reciprocal space.

It is easily seen that the intensity given by Eq. (15) produces satellite reflections exactly at the observed positions shown in Fig. 2(b) by taking $\mathbf{k}_0=[1/3(1+\delta),1/3(1+\delta),3/2]$. It is found that in order to give the quantitative agreement of the incommensurability, the δ value, the interaction parameter should be taken as $-J_4/J_1=0.1$. Notice

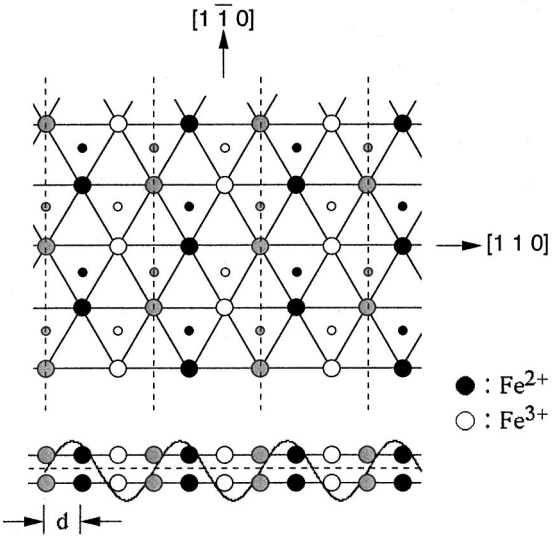

FIG. 8. The local charge-density wave pattern within a double layer where the arbitrary phase factor ϕ is chosen as $\phi=0$. In the more extended region, this pattern is slowly modulated with the period of $(3/\delta')d$.

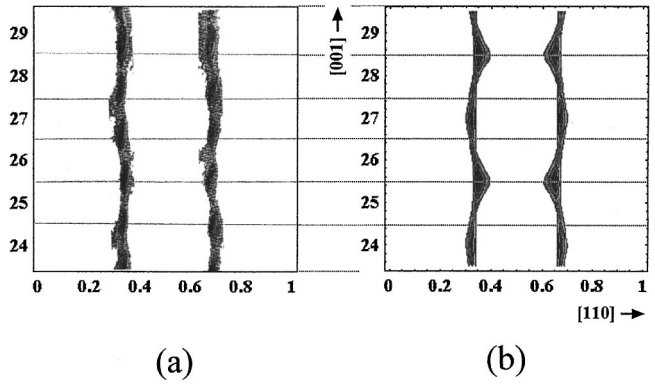

FIG. 9. Comparison of the calculated x-ray diffuse scattering [Eq. (19)] in the (h h l) plane and the observed results. The calculation seems to reproduce the detailed characteristics of the observed zig-zag intensity distribution.

the negative sign means that the fourth-neighbor interaction between the charges is attractive as is pointed out in the preceding section.

B. Polaron fluctuations

Above the transition temperature, the strong diffuse scattering is observed. Definitely, the origin of the diffuse scattering is the correlated fluctuations of polarons. Within the RPA the diffuse scattering due to the critical fluctuation of the order parameter near the phase transition is given by

$$\mathbf{I}_d(\mathbf{K}) \propto \frac{1}{k_B T - J^{\lambda}(\mathbf{k})}, \tag{18}$$

$$\mathbf{K} = \mathbf{K}_h + \mathbf{k},$$

where $J^{\lambda}(\mathbf{k})$ is the Fourier transform of the interaction energy given in Eq. (8). Making use of the definition of the transition temperature given in Eq. (10), we rewrite Eq. (18) in the form

$$\mathbf{I}_d(\mathbf{K}) \propto \frac{1}{k_B(T-T_c) - \{J^{\lambda}(\mathbf{k}) - J^{\lambda}(\mathbf{k}_0)\}}, \tag{19}$$

Equation (19) implies that the diffuse scattering pattern effectively maps out the low-energy contours of $J^{\lambda}(\mathbf{k})$ in the energy range of $J^{\lambda}(\mathbf{k}) - J^{\lambda}(\mathbf{k}_0) \leqslant k_B(T-T_c)$ in the reciprocal space around each Bragg position.

We calculate the diffuse scattering pattern in the (h h l) plane by Eq. (19), where $J^{\lambda}(\mathbf{k})$ given in Fig. 7(c) is utilized. The result is shown in Fig. 9, in comparison with the experimental results. Clearly, the calculated pattern consistently reproduces the observed results including the zig-zag feature.[11]

V. SUMMARY AND DISCUSSIONS

The charge ordering process in a mixed valence system $LuFe_2O_4$ is investigated both experimentally and theoretically. The experimental results using various types of diffraction techniques reveal the following unique features concerning the ordering process. (i) The system undergoes sequential transitions: disorder→2D-CDW→3D-CDW. (ii) The stable structure realized in the lowest temperature is characterized by an incommensurate charge-density wave state having the wave vector $\mathbf{k}_0 = [1/3(1+\delta), 1/3(1+\delta), 3/2]$. (iii) In the intermediate temperature range, there appear strong diffuse streaks running along the rhombohedral unique axis which show subtle zig-zag modulation.

In order to elucidate these unique features a theoretical analysis is carried out based on the assumption that the energy associated with the ordering is given solely by the potential energy between the excess charges. The energy between the electron pairs up to the first-neighbor double layers are taken into account to discuss the ordered configuration of the charges as well as the properties of charge fluctuations above T_c. It has been shown that the experimentally observed unique features of the charge ordering process are satisfactorily explained only when a part of the intercharge interaction between the neighboring double layers is taken to be attractive.

The origin of the attractive interaction would be envisaged as follows. From a macroscopic view point, a charge in the Fe site would induce polarization in the surrounding dielectric medium which may overscreen the core charge at some distance. The charge placed at this distance feels the attractive interaction. Alternatively, from a microscopic viewpoint, we may interpret that since the excess charge on the Fe site tends to induce the displacements of the surrounding oxygen ions to form small polarons, the operator S_i^{υ} in the present treatment is considered to specify the state of polarons, rather than the state of the bare charge and/or hole itself. Accordingly the parameters $J_{ij}^{\upsilon\upsilon'}$ also defines the interaction between the polarons rather than the bare charges. It would not be unphysical to consider attractive interactions between small polarons.

It should be remarked that the postulated 3D-CDW state is not the fully ordered ground state but still contains considerable randomness. This is due to that we have assumed the ordered state in terms of the CDW with a single wave vector, which is valid when the Hamiltonian is strictly defined by the quadratic form Eq. (3). If higher-order energies with respect to the S_i^{υ}'s are taken into account, the ordered state should be expressed generally including the higher harmonics as

$$\rho(\mathbf{r}) = \sum_{n=1}^{\infty} \hat{\rho} \exp[in\mathbf{k}_0 \cdot \mathbf{r} + \phi_n]. \tag{20}$$

One of the experimental evidences of such higher-order effect is seen in the appearance of the higher-order satellite reflections at $(h+3\delta, k+3\delta, l+1/2)$ upon transition. The problem of determining the true ground state is left to future work.

ACKNOWLEDGMENTS

We thank Dr. S. Kito of the Electrotechnical Laboratory for providing excellent single crystals for the present experiments. We thank Dr. S. Mori and Professor N. Yamamoto of the Tokyo Institute of Technology, and Professor Noda, Chiba University for their valuable support in performing electron and x-ray diffraction experiments. This work has been supported by the Institute for Solid State Physics, The University of Tokyo for using the neutron spectrometer at Japan Atomic Energy Research Institute.

[1] N. Kimizuka, E. Muromachi, and K. Shiratori, in *Handbook on the Physics and Chemistry of Rare Earths*, edited by K. A. Gschneidner, Jr. and L. Eyring (Elsevier Science Press, Amsterdam, 1990), Vol. 13, p. 283.

[2] K. Kato, I. Kawada, N. Kimizuka, and T. Katsura, Z. Kristallogr. **143**, 314 (1975).

[3] J. Akimitsu, Y. Inada, K. Shiratori, I. Shindo, and N. Kimizuka, Solid State Commun. **32**, 1065 (1979).

[4] M. Tanaka, H. Iwasaki, K. Shiratori, and I. Shindo, J. Phys. Soc. Jpn. **58**, 1433 (1989).

[5] J. Iida, M. Tanaka, Y. Nakagawa, S. Funahashi, N. Kimizuka, and S. Takekawa, J. Phys. Soc. Jpn. **62**, 1273 (1993).

[6] K. Shiratori, S. Funahashi, J. Iida, and M. Tanaka, Ferrites, *Proceedings of the 6th International Conference on Ferrites* (The Japan Society of Powder and Powder Metallurgy, Kyoto, 1992), p. 703.

[7] N. Ikeda, K. Kohn, H. Kito, J. Akimitsu, and K. Shiratori, J. Phys. Soc. Jpn. **64**, 1371 (1995).

[8] N. Ikeda, K. Saito, K. Kohn, H. Kito, J. Akimitsu, and K. Shiratori, Ferroelectrics **161**, 111 (1994).

[9] N. Ikeda, K. Odaka, E. Takahashi, K. Kohn, and K. Shiratori, Ferroelectrics **190**, 191 (1997).

[10] Y. Yamada, S. Nohdo, and N. Ikeda, J. Phys. Soc. Jpn. **66**, 3733 (1997).

[11] Similar small polaron orders are observed in various hole doped materials such as $La_{1-x}Sr_xMnO_y$ [Y. Yamada *et al.*, Phys. Rev. Lett. **77**, 904 (1996)] and $La_{1-x}Sr_xNiO_7$ [C. M. Chen *et al.*, Phys. Rev. Lett. **71**, 2461 (1993)].